Article

Graphene Oxide Membranes: Controlled Laser Reduction for Sensing Applications

Aiden Rowley, Yijing Stehle *, Luke Kilby and Caleb Bashant

Department Mechanical Engineering, Union College, Schenectady, NY 12308, USA; rowleya@union.edu (A.R.); kilbyl@union.edu (L.K.)
* Correspondence: stehley@union.edu

Abstract: Reduced graphene oxide (rGO) has attracted attention as an active electrode material for flexible electrochemical devices due to its high electric conductivity and large surface area. Compared to other reduction processes, laser reduction is a precise, low-cost, and chemical-free process that is directly applied to graphene oxide (GO) membranes. This study aims to develop rGO through laser irradiation for application as electrodes in thin flexible electrochemical sensors. Laser irradiation parameters will be optimized to achieve reduction of a low oxygen to carbon (O/C) ratio and surface impedance. The influence of humidity on the impedance of rGO electrodes will be studied. The observed instability of the rGO electrode is related to incomplete reduction and oxygenated defects involved in reduction. Partially removed oxygenated functional groups not only influence the impedance of the electrode but make it sensitive to the humidity of the working environment. The result provides references for GO's laser reduction optimization, demonstrates the potential of applying rGO as an electrode in sensing applications, but also reveals the limitation of applying the laser reduced rGO electrode in a non-constant humidity environment.

Keywords: reduced graphene oxide (rGO); graphene oxide (GO); laser reduction; electrode; impedance; humidity sensing

1. Introduction

GO is a monolayer carbon graphene sheet with abundant oxygenated functional groups (OFGs) such as hydroxyl, epoxy, ketone, and carboxyl groups. The OFGs present along the membrane impart electrically insulating and hydrophilic properties of GO. The reduction process of GO involves decomposition and subsequent removal of OFGs in the form of H_2O, CO, and CO_2 from the structure. This causes an increase in conductivity and reduces the hydrophilicity of the GO [1,2]. There are a variety of GO reduction methods ranging from thermal, irradiation, chemical, electrochemical, bacterial degradation, etc. [3–5]. The quality of rGO is limited compared to pristine graphene (unoxidized form) due to incomplete reduction, defects, and chemical residues involved in the reduction process. The application of rGO as a potential electrode material for flexible electrochemical devices and sensors has received attention due to the high electrical conductivity, high specific surface area, and low cost when compared with pristine graphene [6,7]. Compared to chemical and thermal reduction methods, laser-induced reduction of GO (LrGO) has many advantages, such as repeatability, speed, low cost, non-hazardousness, and an automated fabrication process [8,9]. The presence of partially removed OFGs also makes LrGO sensitive to water molecules. Additionally, there are a lack of systematic studies and publications observing the relationship between the laser parameters and the quality of the LrGO, making it difficult to characterize appropriate laser operational settings. Using a high-speed pulse CO_2 laser beam with a wavelength of 10.6 μm, Trusovas et al. [10] determined that a laser power of 50 mW and a scanning speed of 30 mm/s yield optimal reduction results. Alternatively, Dhrubajyoti et al. [11] found that a laser power of 30 W and scanning speed of 10 mm/s

fully reduced a 15 μm GO membrane. Provided that OFGs are a key factor in tailoring electrical resistance and hydrophilicity of GO, the presence of remaining OFGs on the LrGO tends to absorb water vapor molecules in the air. This absorption process impacts the electrochemical performance of the LrGO-based electrochemical supercapacitors and sensors, with working environments of variable humidity. In addition, high-speed pulsed CO_2 lasers tend to generate either foam-like or ablative surface structuring during GO membrane reduction. Combined with the deoxygenation effect, these porous carbon structures serve as an effective electrode candidate for disposable and flexible devices such as supercapacitors and sensors.

In this study, a 200 μm width x 5 cm length LrGO electrode was prepared via a GO membrane (~12 μm thick), with a CO_2 pulse laser beam operating under ambient conditions. Laser parameters including power, scan rate, and focal distance will be optimized to achieve a minimum O/C ratio. The surface morphology and composition of the rGO following laser treatment will be explored via scanning electron microscope (SEM) imaging to further understand the limitations of laser-induced reduction and its effects. Furthermore, the impact of humidity variation on the surface impedance of the rGO electrode will be evaluated in addition to potential sensor applications. Future study will be discussed regarding the application of advanced gold nanoparticles for improved sensitivity.

2. Materials and Methods

Free-standing GO membranes [12] with varying thicknesses between 10 and 16 μm were adhered on flexible substrates with GO solution and left to dry overnight. The GO membrane was reduced using a conventional CO_2 laser engraver (Epilog Fusion Pro, wavelength: 1065 nm) under ambient conditions (21 °C, 30% RH). The surface morphology of the as-prepared pure GO and laser-reduced GO was characterized by Zeiss EVO SEM. The elemental analysis was investigated using Energy Dispersive Spectroscopy (EDS) equipped with SEM. The AC impedance of the LrGO electrode was collected through a four-point probe station using Electrochemistry Impedance Spectra (EIS) (CHI608E) in the frequency range of 1 Hz–0.1 MHz. In the four-point probe station, current was forced through the load via one set of source leads, while the voltage across the load was measured through a second set of leads. To investigate the impact of the humidity of the working environmental on the electric property of the as-prepared rGO electrode, the electrical impedance response to environmental humidity (RH) was measured. This was conducted using saturated salts to produce relatively stable humid environments in an enclosure at a constant temperature of 21 °C [13,14]. To ensure the reliability of the humidity, RH was monitored with a temperature and humidity sensor (Arduino DHT22). The LrGO electrodes were placed into a two-point configuration test mount with two leads attached directly to the electrochemical analyzer, and the impedance was recorded for varying frequencies between 0.01 Hz and 100 kHz at a constant humidity.

3. Results and Discussion

As shown in Figure 1a, the GO membrane surface exhibited a large amount of wrinkle. The "brick-and-mortar" stacking of GO sheets during membrane formation led to 'peak and valley' undulations, which appear as wrinkles on the surface [15]. The surface height variation of the GO membrane due to the wrinkles could result in laser to sample surface distance variation during laser-induced reduction. Laser reduction has its advantage as the only chemical-free, dry, and fast deoxygenation reaction, but also has the disadvantages of incomplete reduction and non-uniformity. In general, laser-induced reduction of GO with a laser wavelength above 800 nm is a photothermal reaction, where local GO flakes are heated above their thermal reduction threshold with the laser beam [16,17]. As shown in Figure 1b, c, two parallel lines separated by a 220 μm distance are directly applied to the GO membrane with a constant laser frequency of 20% and scan speed of 100%. The photothermal and photochemical reduction induced by the laser beam causes the laminated GO sheets to curl up. For laser power below 1 W, only the top few layers of the GO sheet

along the laser beam path curl up, as shown in Figure 1b. The depth of the laser reduction increases with higher laser power. Through optimizing the laser power, frequency, and the planar distance, the resulting LrGO structure (Figure 1c) shows an optimal "bloom", or "raising pastry". The reduction is further confirmed via elemental analysis and resistance measurements. While, visually, the surface of the LrGO appears to be optimal, surface morphology change is not by itself enough to prove that laser irradiation is the most effective reduction method. In our study, the focused laser beam with a smaller diameter generated a large amount of energy on the GO membrane surface to enable instantaneous reduction, which appeared as a "blooming" around the position of the laser dot rather than as uniform exfoliation.
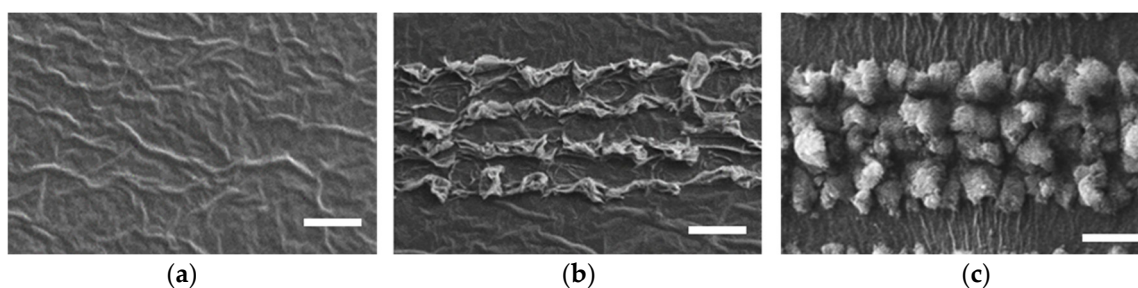

(a) (b) (c)

Figure 1. SEM image of a pristine GO membrane (**a**) under reduced LrGO electrode (**b**) and optimized LrGO electrode (**c**). White scale bars indicate 100 μm.

Further carbon and oxygen elemental maps can be applied to confirm the removal of the oxygenated functional groups. Figure 2 depicts an SEM image and the corresponding energy dispersive x-ray analysis (EDX) maps for carbon (green) and oxygen (blue) at the interface of GO and rGO obtained via line beam irradiation. Comparing the LrGO (bloom) region in Figure 2a with the GO area below it, an oxygen atomic ratio decrease is observed while the carbon atomic ratio does not have a visible difference. It is also observed that 100% reduction is not achieved; there are still plenty of unreduced OFGs present within the GO membrane. This oxygen atomic decrease could greatly influence the effective conductivity of the reduced rGO. The composition is differentiated based on the EDX mapping results. The O/C ratio undergoes significant reduction from the GO region (0.4~0.5) to the rGO region (0.1~0.2), indicating successful laser-induced removal of the majority of the OFGs.
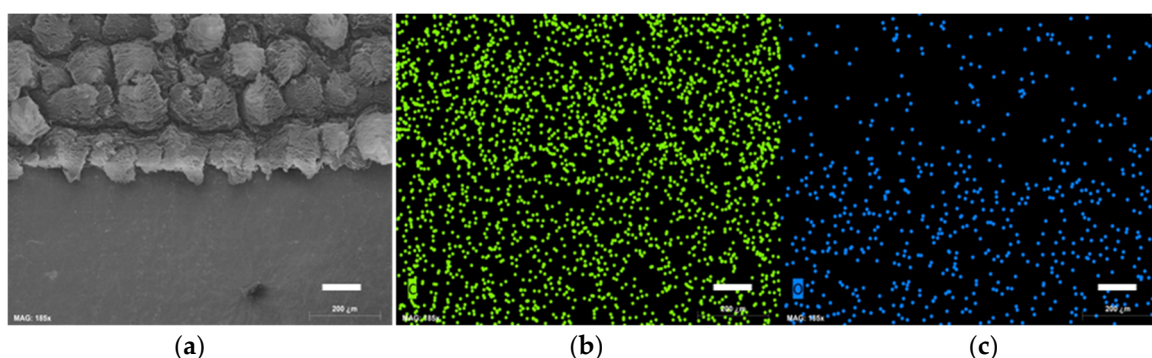

(a) (b) (c)

Figure 2. SEM image (**a**), carbon (**b**), and oxygen (**c**) EDX mapping of an LrGO electrode. White scale bars indicate 200 μm.

The carbon and oxygen element map of GO demonstrates a uniform atom distribution. Upon further observation in Figure 3, a lower carbon concentration and oxygen concentration variation at the location of the laser dot is shown, which indicates non-uniform reduction of the GO due to the nature of the pulse laser. In addition, there is potential carbon removal from overreduction during the laser irradiation process. The hydrophilicity of GO originated from its hydrophilic OFGs, and the removal of OFGs through reduction

processes will decrease its hydrophilicity, as shown in Figure 3d. It is observed that the laser reduction process decreases the hydrophilicity by increasing the average contact angle from 46° to 67° for GO and rGO, respectively. The hydrophilic GO membrane is dispersible in water as GO sheets after sonication, but the LrGO is not dispersible. It is worth mentioning that the hydrophilicity partially contributed to the "bloom" structure of the rGO electrode. There is a large volume increase during the reduction that will increase the porosity of the as-fabricated LrGO electrode. However, the LrGO "bloom" does not hold the same mechanical strength as the GO membrane and can be squeezed through by a gentle push or collected through a brush, which limits the application of the as-fabricated LrGO electrode-based sensor. If the sensing materials' composite with the GO membrane before laser reduction, the sensing materials will undergo "blooming" with the graphene sheet, which could form many nanosized micro-sensors with sensing layers pre-coordinated with the LrGO nanosheets.
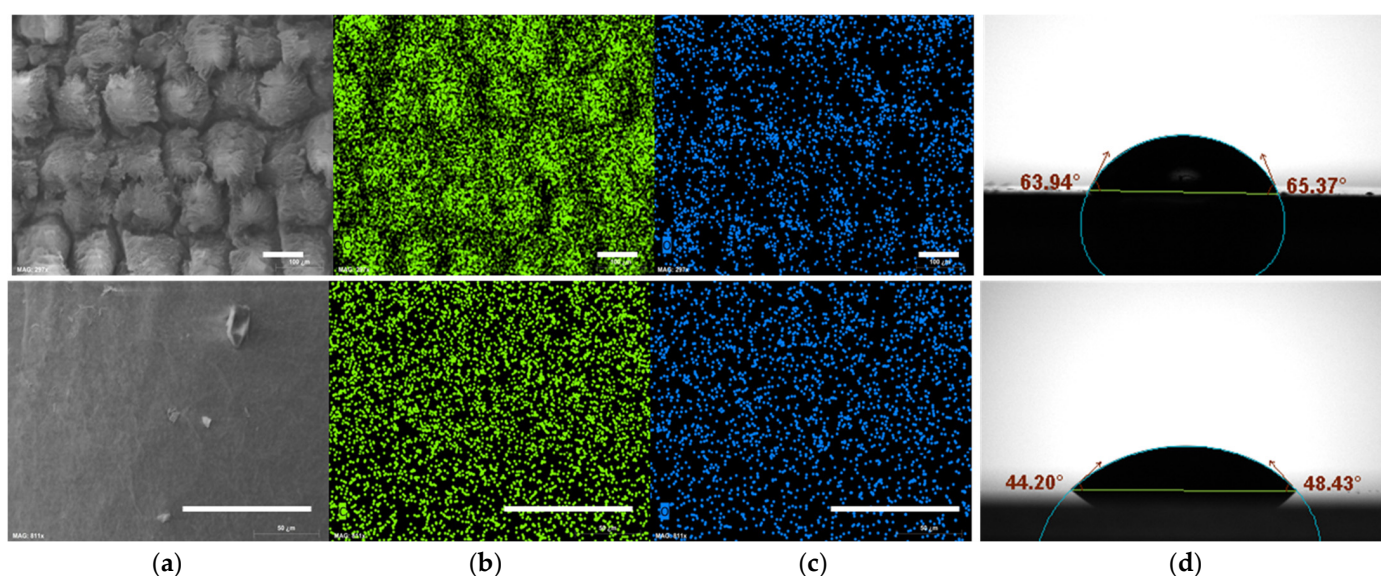

(a) (b) (c) (d)

Figure 3. SEM image (**a**), carbon (**b**), and oxygen (**c**) EDX map, and water contact angle (**d**) of an LrGO electrode (top) and GO membrane (bottom). White scale bars indicate 100 μm (top) and 50 μm (bottom).

With either laser power increase or frequency decrease, the laser beam cuts through the GO membrane directly along its path, rather than inducing and forming a "wrapping" effect through deoxidation. Figure 4 illustrates a typical front view (a) and cross-section view (b) of a laser cut GO membrane, with a corresponding laser power of 3.6 W. Figure 4b demonstrates a membrane thickness increase by a factor of 400 from the GO region to the fully reduced LrGO region when exposed to laser irradiation. Additionally, it is noted that the effective width of laser reduction is limited to within 300 μm. Currently, there is not an effective strategy to form perfect uniform laser reduction of GO membrane on a large area and from top to bottom, which is critical to develop high quality LrGO-based sensors. Therefore, three-dimensional and in situ characterizations of LrGO electrode are needed to better understand the "blooming" mechanism of the GO membrane during the reduction.

As the OFGs on the GO sheet will cut the charge transfer route of the graphene sheet of the GO, the optimized laser reduction should result in the lowest resistance. Here, the Electrochemical Impedance Spectrum (EIS) is applied to evaluate a reduction-induced resistance decrease. The Nyquist plot of an as-prepared LrGO electrode is shown as part of two semicircles. The direct result from EIS was complex impedance ($Z = Z_r + i \cdot Z_i$), which includes both the real part (Z_r) and the imaginary part (Z_i), as shown in Figure 5a. An equivalent circuit inserted in Figure 5a was applied to analyze the effect of laser reduction of the electrode. The equivalent circuit consists of a series resistance, R_s, from the probe connections; interface resistance, R_{ct}, which represents the charge transfer resistivity of the

rGO; and capacitance, C, formed by a rGO/GO/rGO capacitive effect from non-uniform reduction. Figure 5b summarizes the fitted series resistance of the LrGO electrode of the same width and length but with a different laser power and frequency. The longer times and higher temperatures lead to lower resistivity due to the removal of more polymer residue. It was observed that the optimized laser parameter will be 20% frequency, 100% speed, and 2 W power for a 12 µm thick GO membrane.
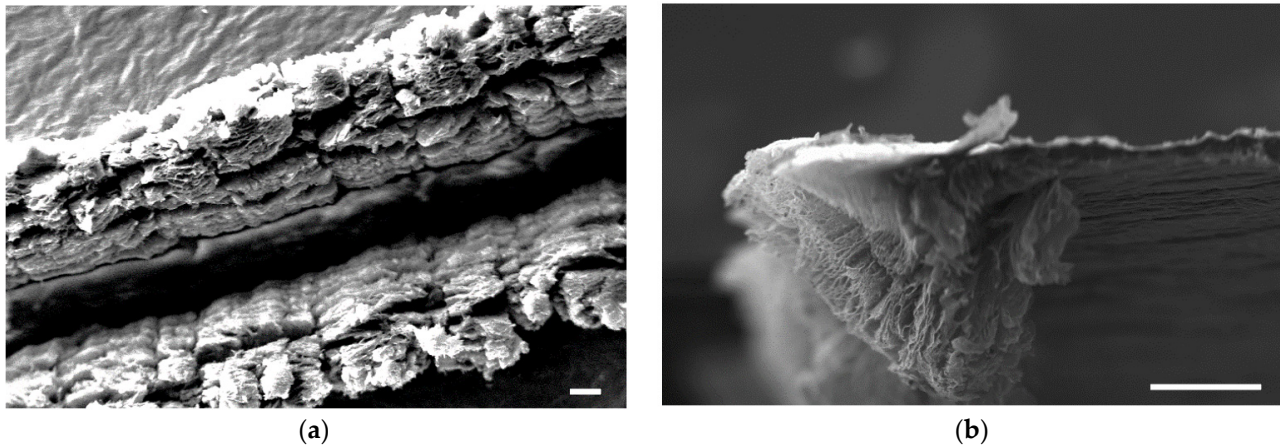

(**a**)   (**b**)

Figure 4. Typical front view (**a**) and cross-section (**b**) SEM image of an LrGO membrane cut. White scale bars indicate 100 µm.

(**a**)   (**b**)
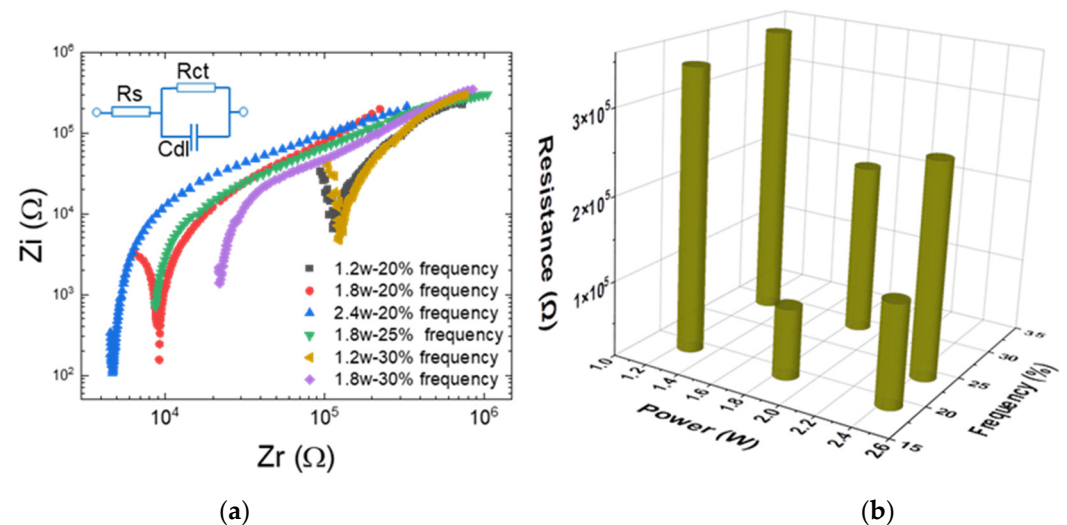
Figure 5. Typical Nyquist plot (**a**) of LrGO electrode reduced with 20% frequency and 1.2 W intensity, a simplified Randles equivalent circuit for impedance fitting; (**b**) relationship between laser power, frequency, and fitted resistance.

The as-prepared LrGO electrode demonstrates promising OFGs removal without overreduction, called "overburn", to the graphene surface of GO. Further power increase either cuts the membrane through or causes burning of the membrane. However, the OFG residue of the LrGO electrode could both lead to water vapor sensitivity and difficulty of recovery following sensing since it will be hard to desorb water after it is bonded with residue OFGs. To evaluate the impact of the humidity of the working environment on the surface impedance of the LrGO electrode, a relative humidity (RH) variation from 30% under ambient condition to 90% under working condition is utilized for a sensing test. Figure 6a shows the impedance of the LrGO electrode as a function of time for a 25 s exposure to a 90% RH working environment, followed by 25 s of recovery. Exposure was under ambient condition (30% RH). It was observed that the total impedance across the

surface of the LrGO electrode decreased 17% over five cycles. While the LrGO electrode responds to humidity change, the impedance drops after working in a high humidity environment, limiting its potential application in a non-dry condition. Similar instability of LrGO is observed in other humidity ranges and temperatures. Such instability from the OFG residue can be solved through either further reduction optimization or by applying sensing layers such as gold nanoparticles above the electrode.
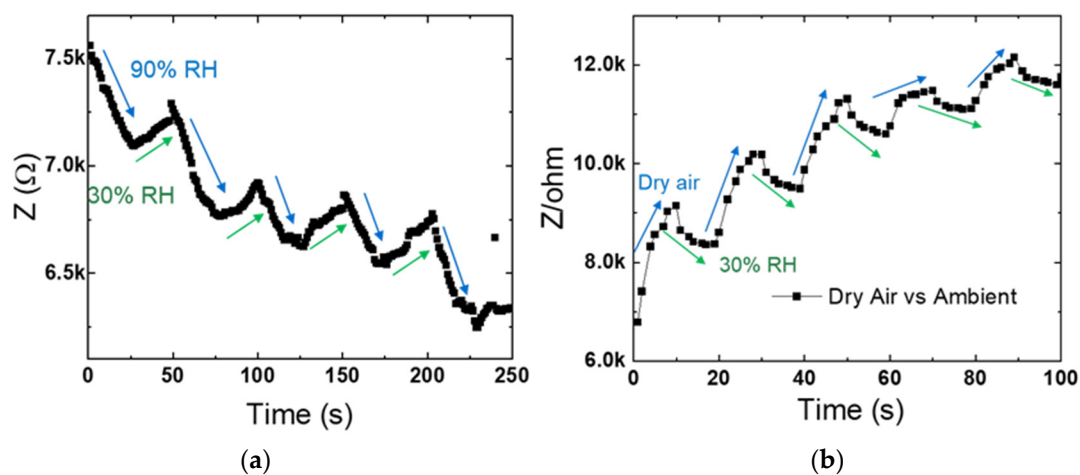

Figure 6. The time–impedance curve of an LrGO electrode exposed to liquid water (**a**) and dry air (**b**) under different humidity environments at room temperature.

The application of LrGO as the electrode in the sensor attracts much attention due to its good electrical conductivity, large surface area, and high stability [17,18]. The humidity sensor made with an LrGO electrode exhibits high sensitivity, stability, reliability, and fast response and recovery in a wide relative humidity (RH) range (11~97%) [19–21]. However, the "bloom" morphology of LrGO represents a non-uniform reduction of the GO membrane. As laser reduction is dependent on the distance from laser tip to the sample surface, the tip of the "bloom" tends to have fewer OFGs than the bottom of the "bloom". Generally, rGO is visualized as hole doped (p-type) semiconductor and charge transport through proton hopping mechanism [22]. As the amount of water adsorbed on the LrGO electrode increases, RH increases and hence the concentration of H^+ ions increase, which will facilitate the proton hopping between hydroxyl groups on the LrGO surface and result in an impedance decrease. In the humidity range of our study, the hydronium ion, H_3O^+, is the major charge carrier, and the charge transport occurs by releasing a proton from each H_3O^+ ion and it bonding to neighboring water molecules, which accept it while releasing another proton by the Grotthuss mechanism [23]. At equilibrium state, the amount of water molecules that physically adsorb and desorb from the LrGO surface is equivalent. As the humidity increases, more water molecules are adsorbed to the LrGO electrode than desorbed until they reach the new equilibrium. The residue OFGs on the LrGO has a tendency to absorb the water molecule, which means it takes a longer time for the LrGO electrode to reach a new equilibrium impedance when switching to a new RH.

Generally, the absorption of water molecules to the carbon surface can be explained with chemisorption and physisorption [24,25]. Chemisorption involves the formation of a chemical bond and is thus difficult to break, while physisorption forms weak van der Waals bonds, and thus physiosorbed water molecules can be easily removed. As shown in Figure 6a, the impedance drop caused by water molecules adsorbed by the LrGO electrode from a high humidity environment is larger than the impedance increases from water molecular desorption after leaving the high humidity range during the same time period. Similarly, in Figure 6b, the impedance increases of the LrGO electrode caused by water molecular desorption when moved to a chamber with dry air humidity is larger than the impedance decreases from slowly absorbing the water molecular back after returning to

the ambient condition. The combination of Figure 6a,b indicates that the slope does not represent the adsorption and desorption rate difference of the LrGO electrode. Instead, it can be considerate as it is easier to interrupt an adsorption/desorption equilibrium than for it to recover after it reaches equilibrium during the humidity change. Such a slope could be a sensing pattern of the LrGO electrode with "bloom "morphology, but more experimental study is needed to better understand its sensing mechanism.

4. Conclusions

In this study, laser-reduced graphene oxide electrodes were fabricated with a CO_2 pulse laser under ambient conditions. The optimized laser irradiation parameter of 2~2.4 W power, 20% frequency, and 100% speed for reducing the GO membrane of 12~16 μm thickness were identified via SEM, EDX, and impedance analyses. The complex impedance of the as-prepared LrGO is fitted through a simplified Randles circuit for valid resistance data. The surface impedance of the as-prepared LrGO electrode is sensitive to the humidity of the working environment and has difficultly recovering after being influenced by the working environment humidity change. The RH%-dependent impedance of the LrGO electrodes impacts their potential application in a non-dry working environment and demonstrates the potential of the LrGO electrode for application as a non-contact sensor. This study promotes the understanding of laser reduction condition optimization and the sensing behavior limitations of LrGO electrodes. Further study on the sensing behavior of LrGO electrode-based sensors with the application of added sensing material will be explored. Under the influence of this complex working environment, a better understanding of the limitations of LrGO and the potential solutions is necessary in future research.

Author Contributions: A.R. methodology, investigation, writing—original draft preparation; Y.S. Conceptualization, methodology, visualization, writing—review and editing, validation; L.K. methodology; C.B. methodology. All authors have read and agreed to the published version of the manuscript.

References

1.　Pei, S.; Cheng, H.-M. The Reduction of Graphene Oxide. *Carbon* **2012**, *50*, 3210–3228. [CrossRef]
2.　He, H.; Riedl, T.; Lerf, A.; Klinowski, J. Solid-State NMR Studies of the Structure of Graphene Oxide. *J. Phys. Chem.* **1996**, *100*, 19735–19739. [CrossRef]
3.　Chua, C.K.; Pumera, M. Chemical Reduction of Graphene Oxide: A Synthetic Chemistry Viewpoint. *Chem. Soc. Rev.* **2014**, *43*, 291–312. [CrossRef] [PubMed]
4.　Lee, S.W.; Mattevi, C.; Chhowalla, M.; Sankaran, R.M. Plasma-Assisted Reduction of Graphene Oxide at Low Temperature and Atmospheric Pressure for Flexible Conductor Applications. *J. Phys. Chem. Lett.* **2012**, *3*, 772–777. [CrossRef]
5.　Cai, J.; Lv, C.; Aoyagi, E.; Ogawa, S.; Watanabe, A. Laser Direct Writing of a High-Performance All-Graphene Humidity Sensor Working in a Novel Sensing Mode for Portable Electronic. *ACS Appl. Mater. Interfaces* **2018**, *10*, 23987–23996. [CrossRef]
6.　El-Kady, M.F.; Kaner, R.B. Scalable Fabrication of High-Power Graphene Micro-Supercapacitors for Flexible and On-Chip Energy Storage. *Nat. Commun.* **2013**, *4*, 1475. [CrossRef]
7.　In, J.B.; Hsia, B.; Yoo, J.-H.; Hyun, S.; Carraro, C.; Maboudian, R.; Grigoropoulos, C.P. Facile fabrication of flexible all solid-state micro-supercapacitor by direct laser writing of porous carbon in polyimide. *Carbon* **2015**, *83*, 144–151. [CrossRef]
8.　Gao, W.; Singh, N.; Song, L.; Liu, Z.; Reddy, A.L.M.; Ci, L.; Vajtai, R.; Zhang, Q.; Wei, B.; Ajayan, P.M. Direct Laser Writing of Mirco-Supercapacitors on Hydrated Graphene Oxide Films. *Nat. Nanotechnol.* **2011**, *6*, 496–500. [CrossRef]
9.　Yang, D.; Bock, C. Laser Reduced Graphene for Supercapacitor Applications. *J. Power Sources* **2017**, *337*, 73–81. [CrossRef]
10.　Trusovas, R.; Ratautas, K.; Račiukaitis, G.; Barkauskas, J.; Stankevičienė, I.; Niaura, G.; Mažeikienė, R. Reduction of Graphite Oxide to Graphene with Laser Irradiation. *Carbon* **2013**, *52*, 574–582. [CrossRef]

11. Bhattacharjya, D.; Kim, C.-H.; Kim, J.-H.; You, I.-K.; In, J.B.; Lee, S.-M. Fast and controllable reduction of graphene oxide by low-cost CO_2 laser for supercapacitor application. *Appl. Surf. Sci.* **2018**, *462*, 353–361. [CrossRef]

12. Stehle, Y.Y.; Robertson, E.; Cortez, R.; Bucinell, R.B.; Vlassiouk, I.V.; Olsson, K.; Kilby, L. Using Al^{3+} to Taylor Graphene Oxide Nanochannels: Impact on Membrane Stability and Permeability. *Membranes* **2022**, *12*, 871. [CrossRef] [PubMed]

13. O'Brien, F.E.M. The Control of Humidity by Saturated Salt Solutions. *J. Sci. Instrum.* **1948**, *25*, 73. [CrossRef]

14. Greenspan, L. Humidity Fixed Points of Binary Saturated Aqueous Solutions. *J. Res. Natl. Bur. Stand A Phys. Chem.* **1977**, *81A*, 89–96. [CrossRef]

15. Shen, X.; Lin, X.; Yousefi, N.; Jia, J.; Kim, J. Wrinkling in Graphene Sheets and Graphene Oxide Papers. *Carbon* **2014**, *66*, 84–92. [CrossRef]

16. Tran, T.X.; Choi, H.; Che, C.H.; Sul, J.H.; Kim, I.G.; Lee, S.-M.; Kim, J.-H.; In, J.B. Laser-induced reduction of graphene oxide by intensity-modulated line beam for supercapacitor applications. *ACS Appl. Mater. Interfaces* **2018**, *10*, 39777–39784. [CrossRef] [PubMed]

17. Orekhov, N.D.; Bondareva, J.v.; Potapov, D.O.; Dyakonov, P.v.; Dubinin, O.N.; Tarkhov, M.A.; Diudbin, G.D.; Maslakov, K.I.; Logunov, M.A.; Kvashnin, D.G.; et al. Mechanism of Graphene Oxide Laser Reduction at Ambient Conditions: Experimental and ReaxFF Study. *Carbon* **2022**, *191*, 546–554. [CrossRef]

18. Zhu, J.; Huang, X.; Song, W. Physical and Chemical Sensors on the Basis of Laser-Induced Graphene: Mechanisms, Applications, and Perspectives. *ACS Nano* **2021**, *15*, 18708–18741. [CrossRef]

19. Ait Lahcen, A.; Rauf, S.; Beduk, T.; Durmus, C.; Aljedaibi, A.; Timur, S.; Alshareef, H.N.; Amine, A.; Wolfbeis, O.S.; Salama, K.N. Electrochemical sensors and biosensors using laser-derived graphene: A comprehensive review. *Biosens. Bioelectron.* **2020**, *168*, 112565. [CrossRef]

20. Zhu, C.; Tao, L.-Q.; Wang, Y.; Zheng, K.; Yu, J.; Xiandong, L.; Chen, X.; Huang, Y. Graphene oxide humidity sensor with laser-induced graphene porous electrodes. *Sens. Actuators B-Chem.* **2020**, *325*, 128790. [CrossRef]

21. Romero, F.J.; Rivadeneyra, A.; Salinas-Castillo, A.; Ohata, A.; Morales, D.P.; Becerer, M.; Rodriguez, N. Design, fabrication and characterization of capacitive humidity sensors based on emerging flexible technologies. *Sens. Actuators B-Chem.* **2019**, *287*, 459–467. [CrossRef]

22. Yuan, W.; Liu, A.; Huang, L.; Li, C.; Shi, G. High-Performance NO_2 Sensors Based on Chemically Modified Graphene. *Adv. Mater.* **2012**, *25*, 766–771. [CrossRef] [PubMed]

23. Miyake, T.; Rolandi, M. Grotthuss mechanisms: From proton transport in proton wires to bioprotonic devices. *J. Phys. Condens. Matter* **2015**, *28*, 023001. [CrossRef] [PubMed]

24. Tulliani, J.-M.; Inserra, B.; Ziegler, D. Carbon-Based Materials for Humidity Sensing: A Short Review. *Micromachines* **2019**, *10*, 232. [CrossRef] [PubMed]

25. Han, M.; Ding, X.; Duan, H.; Luo, S.; Chen, G. Ultrasensitive Humidity Sensors with Synergy between Superhydrophilic Porous Carbon Electrodes and Phosphorus-Doped Dielectric Electrolyte. *ACS Appl. Mater. Interfaces* **2023**, *15*, 9740–9750. [CrossRef] [PubMed]